



Preparation of spheroidized W–Cu pseudo-alloy micropowder with sub-micrometer particle structure using plasma technology

A. V. SAMOKHIN¹, N. V. ALEKSEEV¹, A. A. DOROFEEV¹, A. A. FADEEV¹,
M. A. SINAYSKIY¹, I. D. ZAVERTIAEV¹, Y. V. GRIGORIEV²

1. Institute of Metallurgy and Materials Science, Russian Academy of Sciences,
Moscow 119334, Leninsky prospect 49, Russian;

2. Federal Scientific Research Center “Crystallography and Photonics”,
Russian Academy of Sciences, Moscow 119334, Leninsky prospect 59, Russian

Received 25 August 2022; accepted 6 May 2023

Abstract: The possibility to obtain composite micropowders of the W–Cu system with spherical particles having sub-microscale/nanoscale internal structure was confirmed and studied using the complex multistage approach. Composite W–Cu nanoparticles with core–shell structure (W cores and Cu shells) were produced in plasmochemical synthesis in the first stage. Further spray-drying of the aqueous suspension of the W–Cu nanopowder with sucrose enabled the formation of 25–63 μm microgranules with a yield of 50%. The last step was the treatment of the nanopowder microgranules by a thermal plasma jet, which ensured the production of dense spherical W–Cu particles. The final powder had a spheroidization degree of 90%–95%, a bulk density of up to 8.1 g/cm^3 and a flowability of 12 s/50 g. The contents of impurities in the resulting spherical micropowder were 0.7 wt.% O, 0.02–0.2 wt.% C and 0.03–0.05 wt.% H.

Key words: W–Cu composites; plasmochemical synthesis; granulation; plasma spheroidization; nanoparticles; microgranules; micropowders

1 Introduction

Metal composites of the W–Cu system, also called pseudo-alloys, contain a W phase with a high melting point, high strength, and low thermal expansion coefficient, and contain a Cu phase with high thermal and electrical conductivities [1,2]. These composites are of considerable interest for various technical applications and are used in the production of electrical contacts, electrodes, heat removal elements of powerful electronic devices, and rocket nozzles [1–3]. One new potential application of W–Cu composites is as components in future fusion plants [4–6].

Modern industrial technologies for fabricating

parts from W–Cu composites are based on the impregnation of initial open-porosity W blanks with molten Cu. Liquid-phase sintering of a mixture of W and Cu powders [1–3] is also used.

The physicochemical properties of W and Cu differ significantly; their melting points are 3695 and 1358 K and their crystal structures are BCC and FCC, respectively. The atomic radii of the metals differ by more than 20%, and the values of electronegativity 2.36 for W and 1.9 for Cu are also different.

According to the equilibrium phase diagram, W and Cu do not possess mutual solubility and do not form compounds under any composition. The difference in the properties of the metals leads to the difficulty of obtaining W–Cu composites with

uniform fine-grained structures and high thermal and electric conductivities, especially in the manufacture of complex parts. Therefore, it is relevant to develop new technologies for the manufacture of W–Cu composites.

The use of initial W–Cu powder nanocomposites has a positive effect on the compaction process, which allows the formation of dense W–Cu composites with uniform sub-micrometer and nanoscale structures, high thermal and electric conductivities, and good mechanical strength [7–9]. Nanopowders of the W–Cu system can be produced by various methods [2,10–12], including the reduction of metal oxide compounds mixtures by H₂ in the Ar radio-frequency plasma [13–15] or by electrical explosion of wires [16]. The plasmochemical synthesis of W–Cu nanopowders has several advantages, including a one-step process, the ability to produce nanopowders with different Cu/W ratios, the absence of foreign metal impurities, the absence of by-products, environmental purity, and scalability. State-of-the-art plasma technology allows the establishment of high-performance plants for producing metal nanopowders based on DC plasma torches with capacities reaching several megawatts [17].

Since the early 1980s, new methods for manufacturing complex parts using additive technologies have been developed worldwide. These are based on the layer-by-layer build-up of a powder product following a three-dimensional computer model under the thermal influence of a focused laser or electron-beam radiation [18–21]. Over three decades of development, additive technologies have permitted the industrial production of finished functional products from various metals and alloys. To date, studies have shown the possibility of obtaining dense W–Cu composites [22–25] through selective laser melting (SLM), which is the basis for the creation of production technologies for manufacturing complex-shaped parts from W–Cu composites with the necessary functional properties.

Metal powders used in layer-by-layer component fabrication by additive techniques should have good fluidity and provide the maximum possible particle packing density during powder layer formation process [26,27]. These requirements can be met by using metal powders with spherical particles of 20–60 μm in diameter.

However, composite W–Cu powders with spherical particles are not commercially produced.

Previously, we proposed a method for producing pseudo-alloy micropowders based on a W–Ni–Fe system with a sub-micrometer structure and spherical particles. The method included: (1) plasmochemical synthesis of W–Ni–Fe system nanopowders during the reduction of the metal oxide mixture by the H₂-containing thermal plasma of a DC plasma torch; (2) granulation of the composite W–Ni–Fe system nanopowders in a spray dryer to obtain nanopowder microgranules; (3) classification of microgranules with the preparation of a given size fraction; (4) DC arc plasma spheroidization of the extracted target fraction of microgranules and classification of the spherical particles [28].

The purpose of this study was to experimentally confirm the possibility of obtaining composite micropowders of the W–Cu system with spherical particles having sub-microscale/nanoscale internal structure using the above-mentioned approach.

2 Experimental

2.1 Preparation of W–Cu system nanopowder

The W–Cu nanopowder (20 wt.% Cu) was obtained through processing a mixture of WO₃ and Cu powders in the H₂-containing thermal plasma flow generated in the DC plasma torch with the nominal power of 30 kW. The DC plasma torch had a self-aligning arc length that was fixed by interelectrode inserts. A detailed description of the installation and processes, leading to the formation of nanoparticles in the thermal plasma stream, is presented in Ref. [29].

The initial powder mixture consisted of WO₃ particles with a size of less than 50 μm (TUMELOM LLC, Russia) and PMVD1 Cu particles with a size of less than 5 μm (VMP CJSC, Russia).

Nitrogen, which was part of the plasma-forming and transporting gas, was supplied from an air separation unit, and the O₂ content in N₂ was not more than 0.1 vol.%. To ensure WO₃ reduction, technical-grade H₂ was added to the plasma-forming gas.

2.2 Preparation of W–Cu system nanopowder microgranules

Nanopowder microgranules of the W–Cu

system were obtained using a Buchi Mini Spray Dryer B-290 (Switzerland), equipped with an ultrasonic nozzle, by the spray-drying of aqueous suspensions of the plasma-produced W-Cu nanopowder.

Spray-drying is a widely used method to obtain dense and resistant to mechanical destruction microgranules of a given size range from nanopowders [30]. The preparation of the W-Cu system microgranules using a spray-drying unit comprises three main steps: (1) preparation of an aqueous suspension of composite W-Cu nanoparticles with a sucrose binder; (2) spray-drying of the suspension obtained using an ultrasonic nozzle, during which N_2 was used as the working gas (drying and cooling) in the granulation of the nanopowder along with the Buchi B-295 circulating gas circuit; (3) separation of microgranules after the granulation process to isolate the target fraction of microgranules with particle sizes of 25–63 μm using a Retsch AS 200 sieve machine (Germany).

2.3 Plasma treatment of W-Cu system nanopowder microgranules

The target fraction of nanopowder microgranules with particle sizes of 25–63 μm was treated in an Ar thermal plasma jet such as Ar-3vol.% H_2 , generated in a DC plasma torch. A detailed description of the unit used for the plasma spheroidization of the powder materials used in this study is given in Ref. [31]. After the plasma treatment of the nanopowder microgranules, some nanoparticles were formed by the partial evaporation and subsequent condensation of the granule material. To remove them, a sedimentation method was used in distilled water after ultrasonic dispersal, in which the spheroidized microparticles (“micro”) were isolated from the resulting suspension during precipitation and subsequent vacuum drying, and the nanoparticles (“nano”) were removed with water as a suspension.

2.4 Complex analysis of physicochemical properties of powder materials

Imaging was performed using a scanning electron microscope (SEM, Scios FEI) with energy-dispersive X-ray spectroscopy (EDX) for elemental analysis, a transmission electron microscope (TEM, Osiris FEI), and an Olympus CX31 optical microscope. For statistical image

processing, ImageScope M software was used.

The specific surface areas and porosities of the powders were determined by the Brunauer–Emmett–Teller (BET) method on a TriStar 3000 specific surface analyzer (Micromeritics). The measurement of the total O and N contents was performed on a TC-600 analyzer (LECO). The total carbon content was determined on a CS-600 analyzer (LECO).

The particle size distribution of the micropowder was measured using a laser diffraction particle size analyzer (Mastersizer 2000M, Malvern). Phase analysis was performed on an Ultima-4 X-ray diffractometer (XRD, RIGAKU).

The classification of nanoparticles in the spheroidized micropowders was accomplished by fractional division in liquid through the sedimentation of the post-processing suspension using an ultrasonic disperser (Bandelin Sonopuls HD3100, Germany).

Powder flowability was determined using a calibrated funnel (Hall instrument) and a 50 g stopwatch. Finally, the bulk densities of the powders were determined by the weight method.

2.5 Thermodynamic analysis of processes in WO_3 -Cu- H_2 system at high temperatures

The equilibrium compositions of the W-Cu-O-H system were calculated to estimate the chemical transformation during the interaction of the WO_3 -Cu mixture with the H_2 -containing thermal plasma.

Thermodynamic analysis was performed using the TERRA software complex for the modeling of the phases and chemical equilibria in multi-component systems [32]. The equilibrium compositions of the WO_3 -Cu- H_2 system were calculated for isobaric and isothermal conditions at temperatures of 400–5000 K and a total pressure of 0.1 MPa. In the calculations, the mass ratio of the metals (W/Cu) in the system was 4, and the H/O molar ratios were set to be 2, 4, 8, and 12, corresponding to excessive H contents of 1 (stoichiometric condition), 2, 4, and 6, respectively.

Calculations showed that Cu is present in the system as a metal at temperatures below 2000 K, with a yield of 100% (Fig. 1). The temperature range of the equilibrium 100% yield of metallic W depends on the excess of hydrogen. For H/O molar ratio of 4, W equilibrium with 100% yield occurs

from 1400 to 2100 K. For H/O molar ratios of 8 and 12, it occurs from 1050 to 2700 K and from 950 to 2800 K, respectively (Fig. 1).

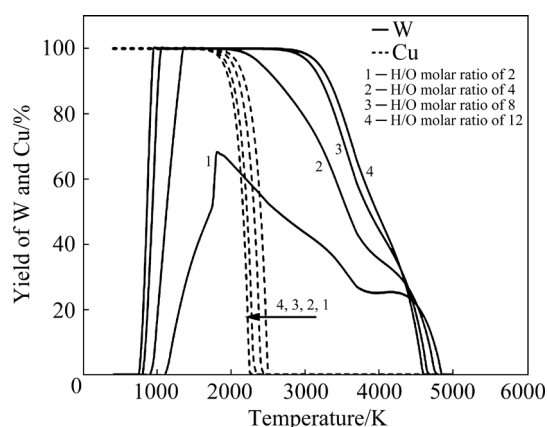


Fig. 1 Dependence of equilibrium yield for W and Cu metals on temperature at different H/O molar ratios

The actual plasmochemical synthesis of nanoparticles from the dispersed raw materials is implemented to ensure the complete evaporation of the raw materials, thereby eliminating contamination of the obtained nanoscale product by impurities of non-evaporated raw materials in the micrometer size range. The formation of nanoparticle products occurs as a result of the chemical condensation of vapors from the gas phase upon cooling the high-temperature stream and reducing the temperature from that at the beginning of condensation to that at which the maximum output of the condensation product occurs. The starting temperature of the W equilibrium condensation for the considered H/O molar ratios is in the range of 4600–4850 K. On decreasing the temperature to 3700 K (the melting point of W), W vapor condenses from 43% (H/O molar ratio of 4) to 65% (H/O molar ratio of 12). The nanoparticles obtained in this temperature range are in the liquid state; therefore, after complete cooling, they have spherical shapes. Under conditions where the temperature decreases below the crystallization temperature of W, nanoparticle formation occurs by the vapor–crystal mechanism and the nanoparticles are faceted. Thus, the resulting W nanopowder was a mixture of spherical and faceted nanoparticles.

The composition of the W-containing components of the gas phase, from which metallic W is formed, varies depending on the temperature (Fig. 2), and is also influenced by the change in the H/O molar ratio. W vapors are present in the

system at temperatures above 4500 K. With a decrease in temperature, the predominant gas-phase W-containing components become WO and then WO₂. The conversion reactions of these components provide the formation of condensed W under the equilibrium cooling conditions of the system.

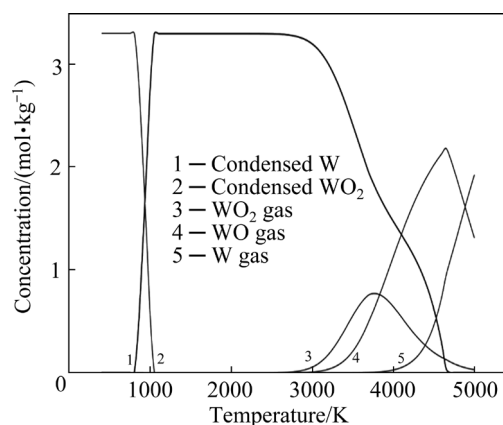


Fig. 2 Dependence of equilibrium concentrations for W-containing components in system at H/O molar ratio of 4

The equilibrium condensation of Cu occurs when the temperature is 2300–2500 K. Beyond these temperatures, Cu is in equilibrium as a metal vapor; therefore, metal formation occurs without the participation of chemical reactions and under conditions where all W is already present in the solid state. When Cu is condensed, W nanoparticles present in the gas capture the Cu atoms and clusters. These form layers of liquid Cu on the surface of the W nanoparticles, yielding W core–Cu shell-structured nanoparticles because Cu and W are not mutually soluble.

3 Results and discussion

3.1 W–Cu composite nanoparticles

The ranges of the process parameters for producing the W–20wt.%Cu nanopowders in the thermal plasma flow generated by the DC plasma torch are listed in Table 1.

The first cycle of experiments was to find a process arrangement that ensured the complete processing of the initial powder mixture WO₃ + Cu. This was achieved by using an Ar–N₂ mixture as a plasma-forming gas and H₂ as a transporting gas to carry the powder mixture from the powder feeder to the plasma flow. The above composition of the

Table 1 Processing parameters for producing nanopowders with W–20wt.%Cu system

Parameter	Parameter value or characteristic description
Input power of plasma torch/kW	19–24
Plasma-forming gas	N ₂ + 25 vol.% H ₂ ; Ar + 30 vol.% N ₂
Plasma-forming gas flow rate/(m ³ ·h ⁻¹)	1.0–4.3
Transport gas	N ₂ ; H ₂ ; N ₂ + H ₂
Transport gas flow rate/(m ³ ·h ⁻¹)	0.3–0.6
Plasma jet enthalpy/(kW·h·m ⁻³)	3.2–8.7
Raw material flow rate/(g·min ⁻¹)	1.5–10

plasma-forming gas provided the maximum plasma flow enthalpy in the plasma torch design, which enabled nearly complete evaporation of the raw material particles to obtain nanopowders containing not more than 2 wt.% of a micrometer-scale size fraction consisting of non-evaporated particles.

The specific surface area of the nanopowders obtained in the experiments varied from 2.8 to 4.7 m²/g. The main parameter of the process affecting the specific surface area was the consumption rate of raw materials; with an increase

in this rate, the specific surface area decreased, accompanying an increase in the content of the “micro” fraction in the resulting nanopowder.

According to the results of the granulometric analysis, as presented in Fig. 3, the obtained experimental batch of W–Cu nanopowder was a polydisperse system consisting of aggregated composite nanoparticles ranging in size from 10 to 250 nm (Fig. 4(a)).

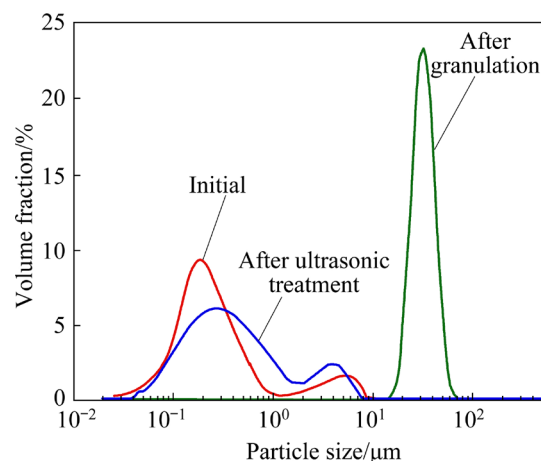


Fig. 3 Results of particle size analysis by static laser diffraction of initial nanopowder, W–Cu granules before ultrasonic treatment and granules after ultrasonic treatment

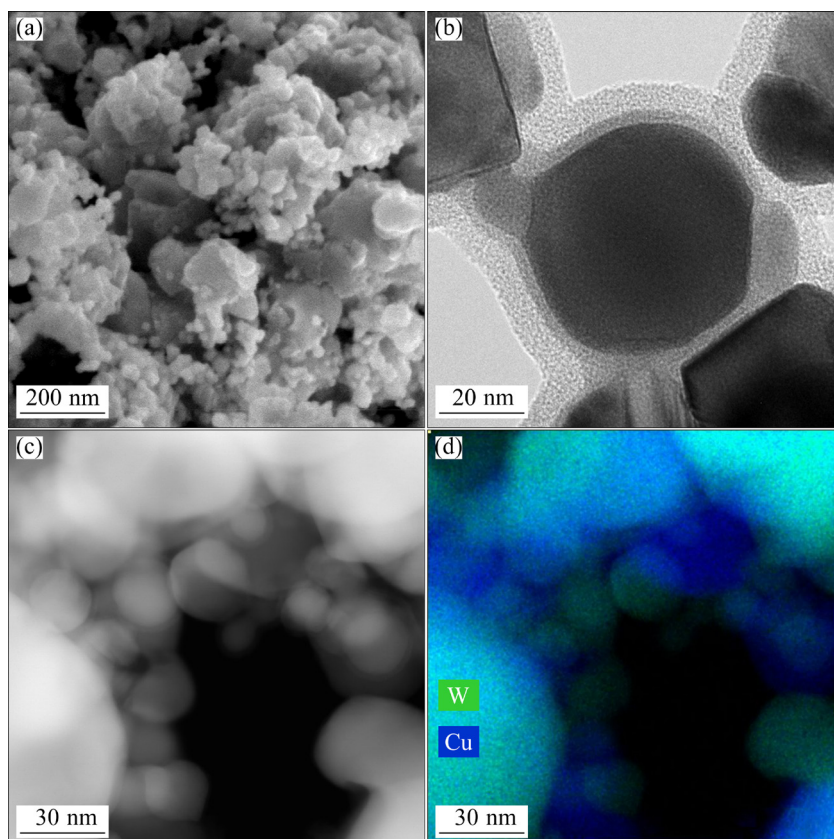


Fig. 4 SEM (a), TEM (b), STEM (c) and TEM–EDX (W + Cu) (d) images of W–Cu nanopowder

Individual nanoparticles have core–shell structures (Fig. 4(b)). The mechanism of nanoparticle formation is described above in the results of thermodynamic calculations. The nanoparticles have either spherical or faceted shapes, which also confirms the conclusions from the thermodynamic model of the process regarding the two formation mechanisms (vapor–liquid–crystal, which yields spheres, and vapor–crystal, which yields faceted particles).

The phase composition of the obtained nanopowder was characterized by the presence of W and Cu metal phases (Fig. 5) uniformly distributed over the volume of the nanopowder, which was confirmed by scanning (SEM–EDX) (Figs. 6(a, b))

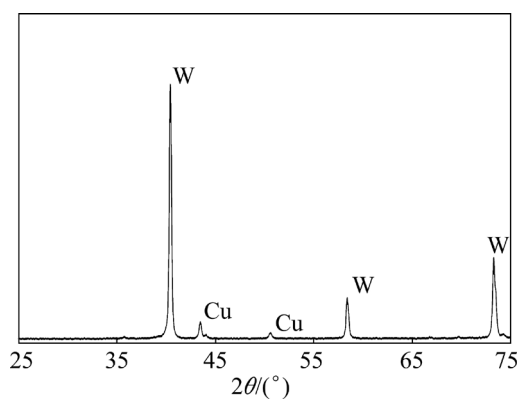


Fig. 5 XRD pattern of obtained W–Cu nanopowder

and transmission (TEM–EDX) electron microscope imaging (Figs. 6(c–e)).

The content of oxygen impurities in the nanopowder ranged from 1.2 to 2.5 wt.%. Because the obtained nanopowder underwent subsequent processing, oxygen impurities can be introduced during some stages, and then the nanopowder contacted the environment. No special measures were taken during plasma chemical synthesis to minimize the oxygen impurity content. The removal of oxygen impurities can be implemented as the final processing stage by the thermochemical treatment of the target powder in a H₂-containing gas medium.

3.2 W–Cu nanopowder microgranules

The parameter variation ranges in the spray-drying unit for the nanopowder granulation process are shown in Table 2.

Sucrose was used as a binder to manufacture suspensions. When sucrose is used in suspension, a high yield of the desired fraction of granules will be achieved. The granules possess sufficient mechanical strength for sowing and transportation during spheroidization from the powder feeder to the plasma stream without destruction; they also show high roundness coefficients without satellites on the surface.

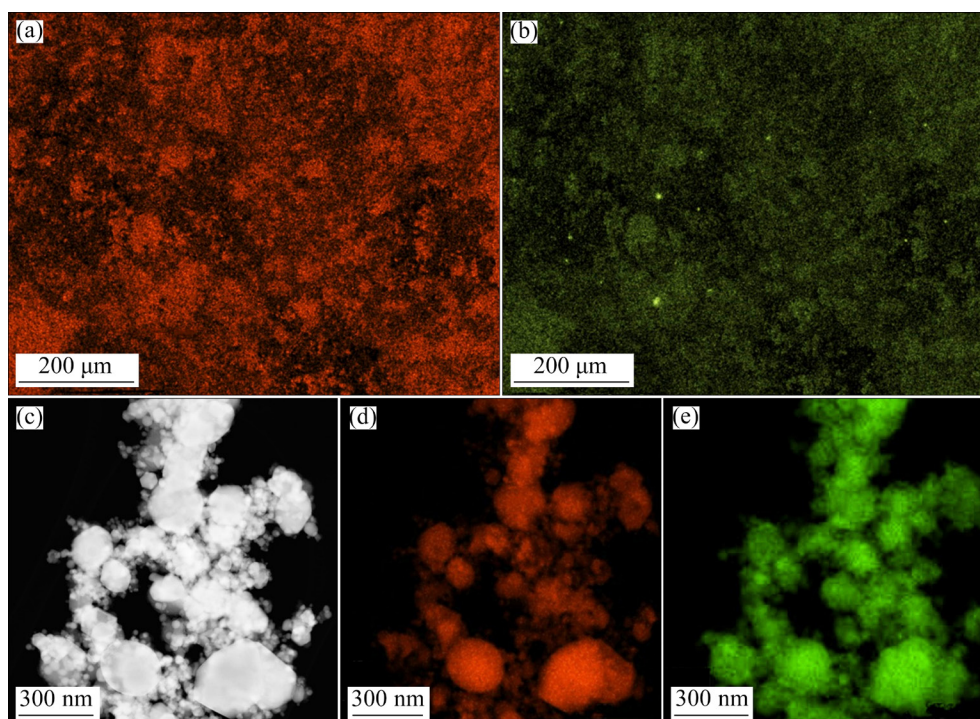


Fig. 6 Images showing distribution of W (a, d) and Cu (b, c) metals in W–Cu nanopowder (SEM–EDX (a, b)) and in individual particles (STEM (c) and TEM–EDX (d, e))

Table 2 Spray-drying parameters and characteristics of nanopowder granulation process

Parameter or characteristic	Parameter value or characteristic description
Drying gas temperature/°C	120–220
Drying gas flow rate/(m ³ ·h ⁻¹)	20
Cooling gas flow rate/(m ³ ·h ⁻¹)	0.4–0.75
Slurry flow rate/(g·min ⁻¹)	2–3
Ultrasonic processing power/W	3
Type of drying chamber	Small with lower outlet without assembly hopper; large with side outlet and assembly hopper
Type of spray nozzle	Ultrasonic

The use of an ultrasonic nozzle in combination with a small drying chamber provides a higher granule yield (approximately 50%) in the size range from 25 to 63 μm because it allows a broader granule size range reaching 60 μm and provides more uniform heating of the chamber itself. The granules outside of this size range can be returned to the granulation process by ultrasonic treatment in water to yield a nanopowder slurry. This operation minimizes the production losses of the nanopowder during granulation (Fig. 3).

The micrograph of the granules prepared using

sucrose as a binder is shown in Fig. 7(a). The granulation experiments of the W–Cu nanopowder by spray-drying an aqueous suspension with 2 wt.% sucrose demonstrated the ability to obtain dense nanopowder granules with an average diameter of 31 μm (Fig. 3). The granules had uniform microstructures without internal cavities (Fig. 7(b)) and uniform distributions of the metals W and Cu (Figs. 7(c, d)). The bulk density of the microgranules was 3.9 g/cm³ and the flowability was 21 s/50 g.

3.3 W–Cu nanopowder microgranules after plasma treatment

The fraction of W–Cu nanopowder microgranules of 25–63 μm in size was processed in the thermal plasma flow of Ar or Ar–3vol.%H₂.

The parameters used for nanopowder microgranule processing in the thermal plasma jet are listed in Table 3.

The thermal plasma jets generated by DC plasma torches are characterized by significant enthalpy and gas velocity gradients. In the plasma jet processing of polydisperse powders, the conditions of the thermal interaction of the treated particles with the high-temperature gas differ. This predisposes possible differences in phase transformations of the particles. Therefore, under

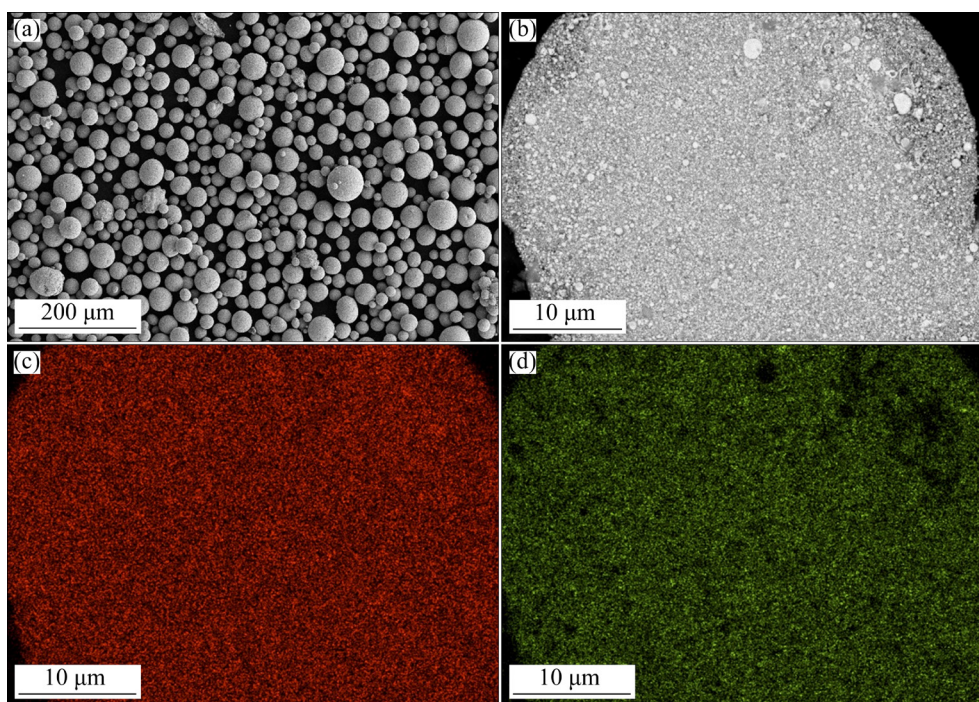


Fig. 7 SEM images of nanopowder granules (a), internal structure of characteristic microgranule after mechanical grinding (b), and SEM–EDX images showing distributions of W (c) and Cu (d)

Table 3 Process parameters for thermal plasma jet treatment of microgranules

Parameter	Value
Input power of plasma torch/kW	15–30
Plasma-forming gas flow rate/(m ³ ·h ⁻¹)	1.5–2.6
Enthalpy of plasma jet/(kW·h·m ⁻³)	0.7–3.7
Transportation flow rate of Ar/(nm ³ ·h ⁻¹)	0.5
Powder flow rate/(g·min ⁻¹)	7–28

these conditions, the treated polydisperse particles can have different internal microstructures. For the densification of a nanopowder, the microgranules must be heated to the melting point of Cu. The heating of metal particles in the high-temperature gas flow is determined by the intensity of heat transfer from the gas to the particle surface. The limited residence time of the microgranules in the high-temperature zone requires the heating of the gas to temperatures well above the boiling point of the particle material to achieve complete melting. The heating and melting of the particles in this case are accompanied by the partial evaporation of the particle material and the subsequent formation of nanosized particles (nanophase); these can adversely affect the use of the powder in practical applications. Owing to the differences in the boiling points of W (5840 K) and Cu (2840 K), the selective evaporation of Cu can occur in the plasma stream, which can cause a change in the chemical composition of the treated material.

Experiments performed in the processing of the W–Cu microgranules in Ar plasma showed that an increase in the enthalpy of the plasma jet in the range from 0.7 to 3.7 kW·h/m³ corresponded to an increase in the nanophase content in the treated powder. The composition of the nanophase was determined by the Cu content. The minimum nanophase content of 1 wt.% was obtained with the plasma jet enthalpy of 0.7 kW·h/m³. For a plasma jet with the enthalpy of 3.7 kW·h/m³, the nanophase accounted for 18 wt.% of the sample and consisted of more than 90 wt.% Cu. An increase in the nanophase content was also observed when treating microgranules in a stream of H₂-containing plasma. This was caused by the increase in the thermal conductivity of the gas and in the heat flux to the microgranules. H₂ reduced the metal oxides present

in the microgranules and thus reduced the total oxygen content of the resulting powder from 2.3 to 1 wt.%.

The treatment of the nanopowder microgranules by the thermal plasma jet ensured their densification, with an increase in powder bulk density from 3.9 to 8.1 g/cm³. Simultaneously, the fluidity was improved to approximately 12 s/50 g. The oxygen content in the powder was decreased during plasma spheroidization from 1.68 wt.% in the nanopowder and 2.15 wt.% in the nanopowder granules to 0.7 wt.% in the spheroidized micropowder. The C content in the spheroidized powder ranged from 0.02 wt.% to 0.2 wt.%. The presence of C was determined by the concentration of the organic binder used in the granulation of the nanoparticles and the enthalpy during the plasma spheroidization process. Finally, the hydrogen impurities were decreased from 0.2 wt.% in the nanopowder granules to 0.03 wt.% in the spheroidized micropowder.

Figure 8(a) shows SEM image of particles after plasma treatment. A microstructural analysis of the internal structure of the particles obtained after plasma treatment indicated the following main types, as shown in Figs. 8(b–e): (1) dense and substantially non-porous structures with sub-micrometer grain size (Fig. 8(b)); (2) porous structures with sub-micrometer-sized pores (Fig. 8(c)); (3) structures with dense cores and shells with sub-micrometer-sized pores (Fig. 8(d)); (4) dense structures with internal cavities (Fig. 8(e)).

The formation of the structure shown in Fig. 8(b) occurs through the fusion of Cu nanoparticles at microgranule temperatures higher than the melting point of Cu, but lower than its boiling point. The structure shown in Fig. 8(c) is formed by heating the microgranules above the boiling point of Cu, but below the melting point of W. In this case, the particle is a porous W matrix from which Cu has almost completely evaporated. The structure shown in Fig. 8(d) is formed during the transition from that shown in Fig. 8(b) to that in Fig. 8(c). It is characterized by the partial evaporation of Cu, and the degree of which is determined by the residence time of the particle in the high-temperature region of the gas stream. The formation of the structure shown in Fig. 8(e) is probably associated with gas

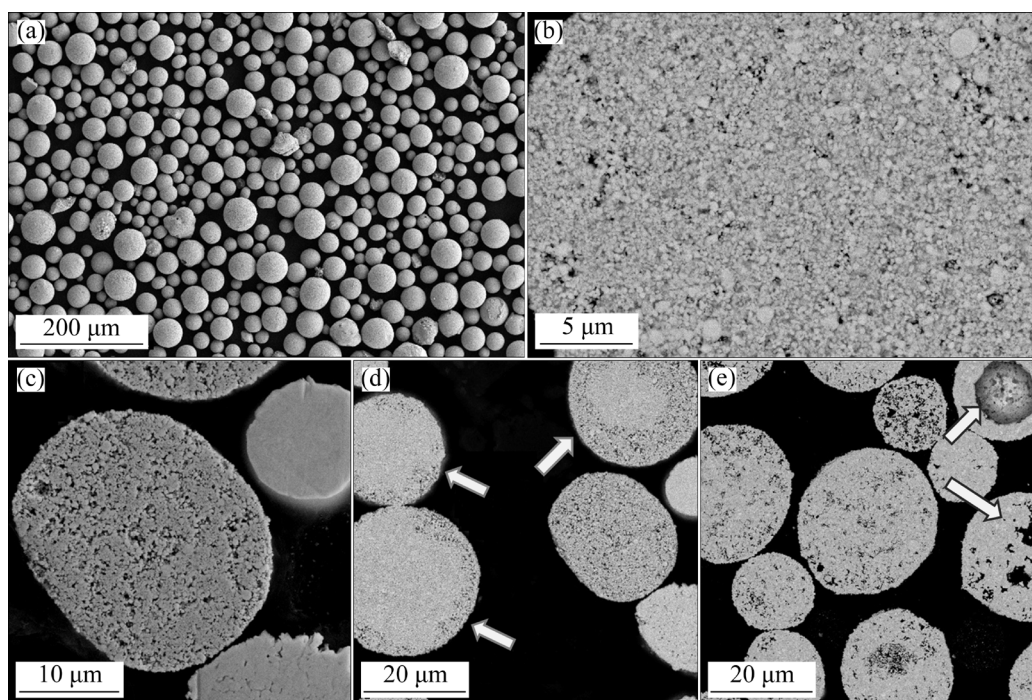


Fig. 8 SEM images of particles after plasma treatment (a) and microparticle cross-sections characterizing resulting internal microstructures (b–e)

release during the decomposition of organic bond molecules during the fastest heating of the granule. In this case, a shell of molten Cu with W particles is formed, and gas is released in the particle core when the organic bonds decompose.

In the all experiments performed, we obtained powders with a particle spheroidization degree of 90%–95% (Fig. 8(a)), which was determined by the near-spherical shape of the original microgranules. The average diameter of the resulting spherical microparticles was approximately 24 μm (Fig. 9).

Based on the results of EDX indicated in Table 4, Cu was evenly distributed over the volume of all microparticles (Figs. 10(a–c)). However, increasing the plasma flow enthalpy induced significant Cu evaporation (Figs. 10(d–f)), which explained the appearance of particles with the structures shown in Figs. 8(c) and (d).

The strong non-isothermal nature of the plasma flow and the difference in size and trajectories of the granules cause the formation of different structures upon thermal plasma jet treatment of the W–Cu nanopowder microgranules. It is difficult to ensure the formation of uniformly structured microparticles, but it is possible to achieve a predominance of the given structure when

optimizing the parameters of the plasma treatment process.

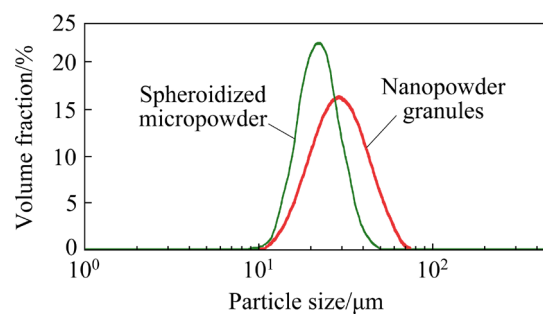


Fig. 9 Results of particle size analysis through laser diffraction of nanopowder granules and spheroidized micropowder

Table 4 Results of EDX microanalysis for samples obtained after plasma treatment with minimal and maximum enthalpy

Sample	Plasma enthalpy/ ($\text{kW}\cdot\text{h}\cdot\text{m}^{-3}$)	Elemental content/wt.%	
		W	Cu
No. 1 micro	0.7	81.2	18.8
No. 2 micro	1.8	90.5	9.5
No. 3 micro	3.7	96.3	3.7
No. 3 nano	3.7	8.7	91.3

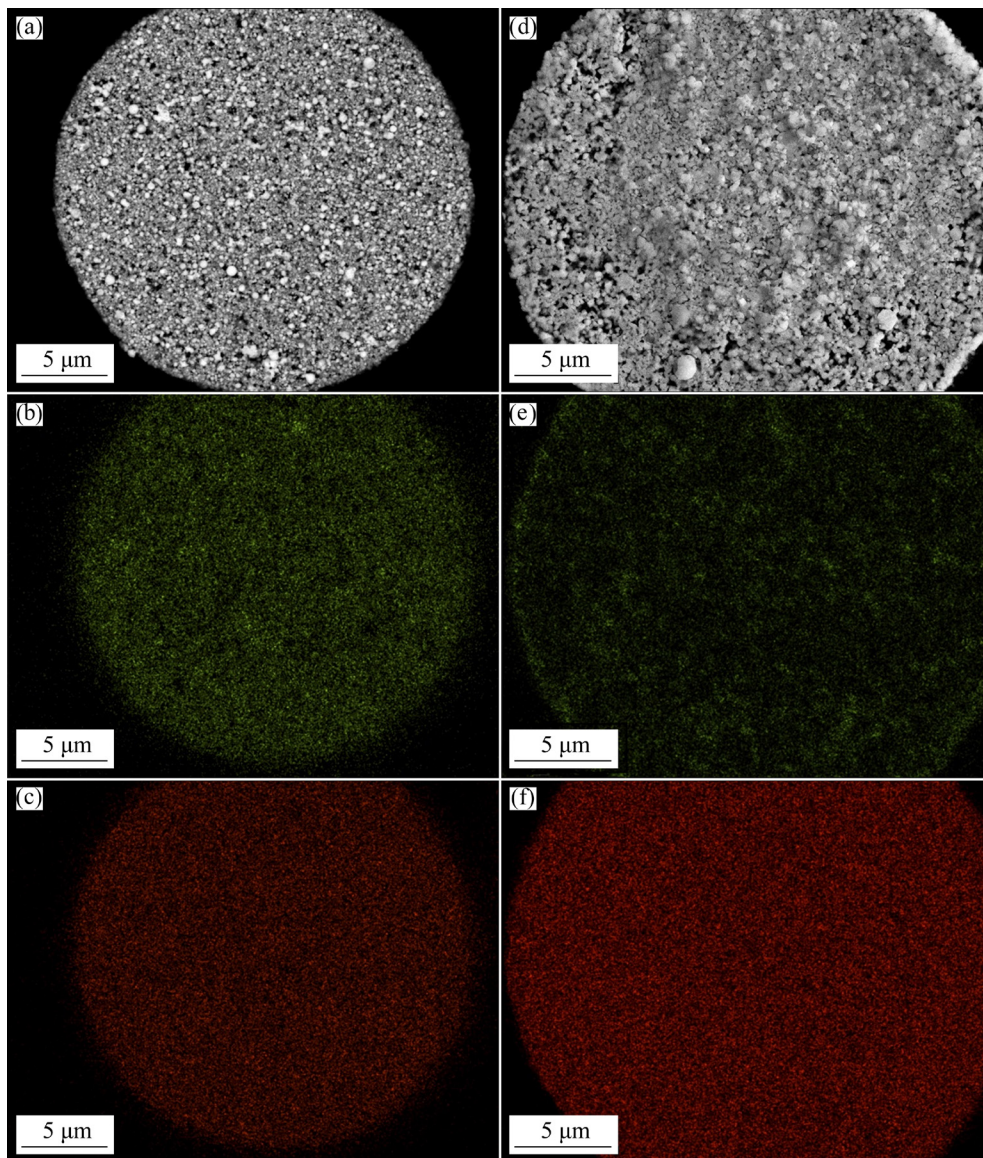


Fig. 10 SEM images of cross-sections of microparticles obtained after plasma treatment with minimum (a) and maximum (d) enthalpy, as well as SEM-EDX distribution maps of Cu (b, e) and W (c, f): (a, b, c) Sample No. 1 micro; (d, e, f) Sample No. 3 micro

4 Conclusions

(1) The fundamental possibility for obtaining of W–Cu (20 wt.%) composite micropowders with spherical particles and sub-micrometer structures for powders of interest in the high-tech additive technologies was demonstrated.

(2) The proposed approach includes three main stages of the process: plasmochemical synthesis of W–Cu nanopowders through the reduction of a metal oxide mixture in H_2 -containing thermal plasma from a DC plasma torch; granulation of composite W–Cu nanopowders by spray-drying to

obtain nanopowder microgranules; DC arc plasma spheroidization of the extracted target fraction of the microgranules.

(3) Composite W–Cu nanoparticles produced in plasmochemical synthesis had core–shell structures with W cores and Cu shells. Spray-drying of the aqueous suspension consisting of the W–Cu nanopowder with sucrose binder enabled the formation of mechanical strength microgranules with a characteristic size of 25–63 μm and 50% yield. The treatment of the nanopowder microgranules by a thermal plasma jet ensured the production of spherical W–Cu particles. The final powder had a spheroidization degree of 90%–95%,

a bulk density reaching 8.1 g/cm³ and a flowability of 12 s/50 g. The contents of impurities in the resulting spherical micropowders were 0.7 wt.% O, 0.02–0.2 wt.% C and 0.03–0.05 wt.% H.

(4) The particles obtained after plasma treatment had sub-micrometer structure with various morphologies, determined by the conditions of thermal interaction of the initial microgranules with the thermal plasma flow.

CRedit authorship contribution statement

A. V. SAMOKHIN: Conceptualization, Supervision, Funding acquisition, Writing original draft; **N. V. ALEKSEEV:** Methodology, Software, Resources, Writing original draft; **A. A. DOROFEEV:** Formal analysis, Investigation, Writing original draft, Project administration; **A. A. FADEEV:** Validation, Investigation, Writing – Review & editing; **M. A. SINAYSKIY:** Investigation, Resources, Writing – Review & editing, Visualization; **I. D. ZAVERTIAEV:** Software, Formal analysis; **Y. V. GRIGORIEV:** Resources.

Declaration of competing interest

The authors declare that they have no known competing financial interests or personal relationships that could have appeared to influence the work reported in this paper.

Acknowledgments

The study was funded by a grant of Russian Science Foundation (<https://rscf.ru/en/project/22-19-00112/>).

References

- [1] DONG L L, AHANGARKANI M, CHEN W G, ZHANG Y S. Recent progress in development of tungsten–copper composites: Fabrication, modification and applications [J]. *International Journal of Refractory Metals and Hard Materials*, 2018, 75: 30–42. <https://doi.org/10.1016/j.ijrmhm.2018.03.014>.
- [2] DONG L L, CHEN W G, HOU L T, DENG N, ZHENG C H. W–Cu system: Synthesis, modification, and applications [J]. *Powder Metallurgy and Metal Ceramics*, 2017, 56: 171–184. <https://doi.org/10.1007/s11106-017-9884-6>.
- [3] ERCETIN A, ASLANTAS K. Production of W–Cu electrical contact material via conventional powder metallurgy method: Characterization, mechanical and electrical properties [J]. *Turkish Journal of Nature and Science*, 2017, 6: 37–42.
- [4] TEJADO E. W–Cu metal matrix composites for next generation fusion devices [J]. *Materials Today*, 2020, 38: 136–137. <https://doi.org/10.1016/j.mattod.2020.07.001>.
- [5] COENEN J, RIESCH J, YOU H. Tungsten composite materials for fusion first wall applications [C]/Proceedings of the IAEA Fusion Energy Conference. Kyoto, Japan, 2016.
- [6] CHONG F L. Development of W/Cu plasma facing component for fusion device [J]. *Materials Science Forum*, 2015, 809/810: 750–756. <https://doi.org/10.4028/www.scientific.net/MSF.809-810.750>.
- [7] HOU C, SONG X Y, TANG F W, LI Y R, CAO L J, WANG J, NIE Z R. W–Cu composites with submicron- and nano-structures: Progress and challenges [J]. *NPG Asia Materials*, 2019, 11: 74. <https://doi.org/10.1038/s41427-019-0179-x>.
- [8] FAN J L, LIU T, ZHU S, HAN Y. Synthesis of ultrafine/nanocrystalline W–(30–50)Cu composite powders and microstructure characteristics of the sintered alloys [J]. *International Journal of Refractory Metals and Hard Materials*, 2012, 30: 33–37. <https://doi.org/10.1016/j.ijrmhm.2011.06.011>.
- [9] TSAKIRIS V, LUNGU M, ENESCU E, PAVELESCU D, DUMITRESCU G, RADULIAN A, MOCIOI N. Nanostructured W–Cu electrical contact materials processed by hot isostatic pressing [J]. *Acta Physica Polonica A*, 2014, 125: 348–352. <https://doi.org/10.12693/APhysPolA.125.348>.
- [10] CHEN A Q, HUO W T, DONG L L, CHEN W G, ZHOU Y. Recent advance of copper tungsten composite materials [J]. *Materials China*, 2021, 40(2): 152–160. <https://doi.org/10.7502/j.issn.1674-3962.202002006>.
- [11] WANG Y L, ZHUO L C, YIN E H. Progress, challenges and potentials/trends of tungsten–copper (W–Cu) composites/pseudo-alloys: Fabrication, regulation and application [J]. *International Journal of Refractory Metals and Hard Materials*, 2021, 100: 105648. <http://dx.doi.org/10.1016/j.ijrmhm.2021.105648>.
- [12] LUNGU M V. Synthesis and processing techniques of tungsten copper composite powders for electrical contact materials: A review [J]. *Oriental Journal of Chemistry*, 2019, 35(2): 491–515. <http://dx.doi.org/10.13005/ojc/350201>.
- [13] OH J W, NA H, CHO Y S, CHOI H. In situ synthesis of bimetallic tungsten–copper nanoparticles via reactive radio-frequency (RF) thermal plasma [J]. *Nanoscale Research Letters*, 2018, 13: 220. <https://doi.org/10.1186/s11671-018-2623-1>.
- [14] KOBAYASHI N, KAWAKAMI Y, KAMADA K, LI J G, WATANABE T, ISHIGAKI T. Spherical submicron-size copper and copper–tungsten powders prepared in RF induction thermal plasma [J]. *Journal of the Japan Society of Powder and Powder Metallurgy*, 2007, 54: 39–43. <https://doi.org/10.2497/jjspm.54.39>.
- [15] LI X J, HU P, WANG J S, CHEN S Q, ZHOU W Y. In situ synthesis of core–shell W–Cu nanopowders for fabricating full-densified and fine-grained alloys with dramatically improved performance [J]. *Journal of Alloys and Compounds*, 2021, 853: 156958. <https://doi.org/10.1016/j.jallcom.2020.156958>.
- [16] PERVIKOV A V, LOZHKOMOEV A S, DVILIS E S. Synthesis of W–Cu composite nanoparticles by the electrical explosion of two wires and their consolidation by spark plasma sintering [J]. *Materials Research Express*, 2019, 6(12): 1265i9. <http://dx.doi.org/10.1088/2053-1591/ab715b>.

- [17] ZHUKOV M F, ZASYPKIN A P, TIMOSHEVSKY A N. Electric arc generators of low temperature plasma [M]. Nauka: Novosibirsk, 1999. (in Russian)
- [18] BANDYOPADHYAY A, BOSE S. Additive manufacturing [M]. 2nd ed. New York: CRC Press, 2019.
- [19] FROES F H, BOYER R. Additive manufacturing for the aerospace industry [M]. Amsterdam: Elsevier, 2019.
- [20] MILEWSKI J O. Additive manufacturing of metals: From fundamental technology to rocket nozzles, medical implants, and custom jewelry [M]. Berlin: Springer, 2017.
- [21] LOGACHEVA A I, SENTYURIN J A, LOGACHEV I A. Additive manufacturing technology responsible products from metals and alloys [J]. Perspective Materials, 2015, 5: 5–15. (in Russian)
- [22] TAN C L, ZHOU K S, KUANG T C. Selective laser melting of tungsten-copper functionally graded material [J]. Materials Letters, 2019, 237: 328–331. <https://doi.org/10.1016/j.matlet.2018.11.127>.
- [23] LI R D, SHI Y S, LIU J H, XIE Z, WANG Z G. Selective laser melting W–10wt.%Cu composite powders [J]. The International Journal of Advanced Manufacturing Technology, 2010, 48: 597–605. <https://doi.org/10.1007/s00170-009-2304-4>.
- [24] SONG C H, YANG Y Q, LIU Y, LUO Z Y, YU J K. Study on manufacturing of W–Cu alloy thin wall parts by selective laser melting [J]. The International Journal of Advanced Manufacturing Technology, 2015, 78: 885–893. <https://doi.org/10.1007/s00170-014-6689-3>.
- [25] GU D D, SHEN Y F, WU X J. Formation of a novel W-rim/Cu-core structure during direct laser sintering of W–Cu composite system [J]. Materials Letters, 2008, 62: 1765–1768. <https://doi.org/10.1016/j.matlet.2007.09.087>.
- [26] QIAN M. Metal powder for additive manufacturing [J]. JOM, 2015, 67: 536–537. <https://doi.org/10.1007/s11837-015-1321-z>.
- [27] SAHEB S H, DURGAM V K, CHANDRASHEKHAR A. A review on metal powders in additive manufacturing [C]//Proceedings of the Third International Conference on Inventive Material Science Applications. Coimbatore, India, 2020. <https://doi.org/10.1063/5.0026203>.
- [28] SAMOKHIN A V, FADEEV A A, ALEKSEEV N V, TSVETKOV Y V. Tungsten-based pseudoalloy powder and method of its production: Russian patent, RU2707455C1 [P]. 2019–11–26.
- [29] SAMOKHIN A, ALEKSEEV N, SINAYSKIY M, ASTASHOV A, KIRPICHEV D, FADEEV A, TSVETKOV Y, KOLESNIKOV A. Powder Technology [M]. Berlin: Springer, 2018. <https://doi.org/10.5772/intechopen.76262>.
- [30] NANDIYANTO A B D, OKUYAMA K. Progress in developing spray-drying methods for the production of controlled morphology particles: From the nanometer to submicrometer size ranges [J]. Advanced Powder Technology, 2011, 22: 1–19. <https://doi.org/10.1016/j.apt.2010.09.011>.
- [31] SAMOKHIN A V, FADEEV A A, ALEKSEEV N V, SINAYSKY M A, SUFIYAROV V S, BORISOV E V, KORZNIKOV O V, FEDINA T V, VODOVOZOVA G S, BARYSHKOV S V. Spheroidization of Fe-based powders in plasma jet of DC arc plasma torch and application of these powders in selective laser melting [J]. Inorganic Materials: Applied Research, 2020, 11: 579–585. <https://doi.org/10.1134/S2075113320030417>.
- [32] TRUSOV B G. Software system modeling phase and chemical equilibria at high temperatures [J]. Engineering Journal Science and Innovation, 2012, 2: 240–249. (in Russian)

等离子体技术制备具有亚微米颗粒结构的球化 W–Cu 伪合金微粉

A. V. SAMOKHIN¹, N. V. ALEKSEEV¹, A. A. DOROFEEV¹, A. A. FADEEV¹,
M. A. SINAYSKIY¹, I. D. ZAVERTIAEV¹, Y. V. GRIGORIEV²

1. Institute of Metallurgy and Materials Science, Russian Academy of Sciences,
Moscow 119334, Leninsky prospect 49, Russian;

2. Federal Scientific Research Center “Crystallography and Photonics”,
Russian Academy of Sciences, Moscow 119334, Leninsky prospect 59, Russian

摘要: 采用复杂多级方法研究并证实制备具有亚微米/纳米级内部结构的球形 W–Cu 复合微粉的可能性。首先, 采用等离子体化学合成法制备具有核壳结构的 W–Cu 纳米粉末(W 核及 Cu 壳)。然后, 将 W–Cu 纳米粉末与蔗糖的水悬浮液进行喷雾干燥, 形成 25~63 μm 的微粒, 收率为 50%。最后, 用热等离子体射流处理由纳米粉末组成的微粒, 形成致密的球形 W–Cu 颗粒。成品粉末的球化度为 90%~95%, 体积密度为 8.1 g/cm³, 流动性约为 12 s/50 g, 杂质中 O、C 和 H 的含量(质量分数)分别为 0.7%、0.02%~0.2 %和 0.03%~0.05%。

关键词: W–Cu 复合材料; 等离子体化学合成; 造粒; 等离子体球化; 纳米颗粒; 微粒; 微粉

(Edited by Wei-ping CHEN)